Production of proton-rich isotopes of Pu, Cm, Bk, Ds, Fl, Cn by fusion evaporation reactions with ^{40}Ar projectile[*]

Qing-Qing Yao,[1] Tian-Liang Zhao,[1] and Xiao-Jun Bao[1,†]

[1] *Department of Physics, Collaborative Innovation Center for Quantum Effects, and Key Laboratory of Low Dimensional Quantum Structures and Quantum Control of Ministry of Education, Hunan Normal University, Changsha 410081, People's Republic of China*

The evaporation residual cross sections (ERCSs) of these reaction systems were calculated by bombarding ^{144}Sm, ^{160,164}Dy, ^{165}Ho, ^{166}Er, ^{169}Tm, ^{171,174}Yb, ^{175}Lu, $^{176-180}$Hf, ^{181}Ta, ^{180,182}W and ^{187}Re targets with ^{40}Ar projectile in the theoretical framework of the dinuclear system (DNS) model. The de-excitation process of the compound nuclei is theoretically calculated using two different statistical models, namely the statistical model 1 and statistical model 2 (GEMINI++ model). The calculated ERCSs were also compared with the experimental data. The ERCSs of synthesizing new proton-rich nuclides are investigated based on the fusion evaporation reaction. Predictions were made for the ERCSs of new isotopes of Pu, Cm and Bk in the heavy nuclei region, while the new isotopes of Ds, Cn and Fl are predicted in the superheavy nuclei region of Z≥104.

Keywords: Dinuclear system model, Eevaporation residue cross section, Proton-rich nuclides

I. INTRODUCTION

The synthesis of new elements and nuclides is a popular topic in nuclear physics field [1–3]. It is not only of great significance for understanding the structure of matter, but also provides important information for understanding the evolution of the celestial environment, making it an essential means of exploring nature. Heavy-ion fusion evaporation (FE) reaction play a crucial role in exploring the synthesis of new elements and nuclides [3–12]. In such reactions, heavy ions are accelerated by a heavy-ion accelerator and collide with target nuclei, leading to nuclear fusion and subsequent evaporation processes, which result in the synthesis of new nuclides.

The FE reaction has made great progress in experiment. In 1975, ^{40}Ar beams with energies up to 225 MeV from the Dubna U-300 cyclotron bombarded ^{204}Pb and ^{206}Pb targets and ^{242}Fm was synthesized [13]. The ^{206}Pb and ^{209}Bi targets was bombarded with ^{40}Ar beam from the GSI Universal Linear Accelerator (UNILAC) accelerator to form ^{243}Fm and ^{247}Md in the FE reactions in 1981 [14]. Similarly, the successful synthesis of new nuclides, ^{245}Md and ^{246}Md, was achieved via ^{40}Ar + ^{209}Bi combination at GSI Laboratory in 1996 [15]. An enriched ^{204}Pb target was bombarded with ^{40}Ar beams from the GSI UNILAC accelerator forming ^{241}Fm in the (3n) FE reaction in 2008 [16]. The new neutron deficient isotope ^{217}U was produced in the bombardment of the ^{182}W target with ^{40}Ar ions and identified using a recoil-α-α correlation method in 2000 [17]. In addition, China has also made some achievements in the synthesis of new nuclides by using ^{40}Ar in recent years, such as the team of the Institute of Modern Physics of the Chinese Academy of Sciences (IMPCAS) successfully synthesized the new uranium isotopes ^{215,216}U using the projectile-target combination ^{40}Ar + ^{180}W in 2015 [18, 19]. Since 2017, the IMPCAS has devoted itself to the synthesis and study of Np radioisotopes, and has successively synthesised a series of new neutron-deficient isotopes ^{220,223,224} Np through the FE reactions ^{40}Ar + ^{185,187}Re [20–22]. Recent results from Dubna for the ^{40}Ar + ^{238}U reaction [23] demonstrated that ^{40}Ar beam can also be used for the synthesis of superheavy nucleus.

In the theoretical study, many models have been developed to understand the formation mechanism of heavy and superheavy nuclei in the FE reactions [24–28]. This work is based on the dinuclear system (DNS) model [29–32]. The synthesis of heavy and superheavy nuclei is a complex dynamic process, involving mainly competition between fusion and quasi-fission. The fusion and quasi-fission processes can be viewed as the evolution of the DNS model along the two main degrees of freedom: the relative motion of nuclei in the interaction potential for the formation of DNS and the decay of the DNS (quasi-fission process) along the elongation degree of freedom (internuclear motion); the transfer of nucleons between two nuclei in the mass asymmetric coordinate system $\eta = \frac{A_1 - A_2}{A_1 + A_2}$, which is the process of diffusion of the excited system and leading to the formation of compound nuclei (CN). It is assumed that the two contacting nuclei always maintain their ground state characteristics in the DNS [33–35]. In fact, the nuclei in the DNS are gradually deformed by the strong nuclear and Coulomb interactions between them. And this deformation will alter the masses of nuclei as well as the interactions between them, which will affect the further evolution of the system [36]. So it is usually not negligible. The concept of DNS must, therefore, be improved by decreasing the approximation used to simplify the calculation. In this paper, we numerically investigate the time-dependent dynamical deformations of the interacting nuclei, which are coupled with nucleon transfer the nucleon transfer in the heavy-ion fusion reaction to form superheavy nuclei (SHN). In Ref. [37], it was mentioned that in addition to the asymmetry degree variables of neutrons and protons, the quadrupole deformation of interacting nuclei is also taken as a dynamic variable and construct a new four-variable master equations (MEs). This means that the deformation and the nucleon transfer are

* The National Natural Science Foundation of China (Grants No.12175064, U2167203). Hunan Outstanding Youth Science Foundation (2022JJ10031).

† Corresponding author, baoxiaojun@hunnu.edu.cn

always regarded as a diffusion process controlled by the master equation in the potential energy surface (PES) of the system.

Theoretical calculations were performed using the combination of the DNS + statistical model 1, as well as the combination of the DNS + statistical model 2 (GEMINI++ model). The evaporation residual cross sections (ERCSs) for FE reactions were calculated by bombarding ^{144}Sm, ^{160,164}Dy, ^{165}Ho, ^{166}Er, ^{169}Tm, ^{171,174}Yb, ^{175}Lu, $^{176-180}$Hf, ^{181}Ta, ^{180,182}W and ^{187}Re targets with ^{40}Ar projectile and the results were compared with available experimental data. The article is organized as follows. In Sec. II we give a brief description of the theoretical framework. Results and discussion are presented in Sec. III. Summary is concluded in Sec. IV.

II. THEORETICAL FRAMEWORK

In theoretical studies, it is possible to divide the fusion-evaporation reaction process in more detail into three successive phases. The first phase is the capture process which can be evaluated by the capture cross section; the second phase is the evolution of the DNS from the contact configuration to the formation of compound nucleus which can be evaluated by the fusion probability; the final stage involves the excited compound nucleus undergoing evaporation of light particles to prevent fission and it can be evaluated by the survival probability. Finally, a small ERCS is obtained for the generation of residual nuclei. In the DNS concept, the ERCS is calculated as the sum of all partial waves [24, 25, 38].

$$\sigma_{\mathrm{ER}} = \sum_J \sigma_{\mathrm{cap}}(E_{\mathrm{c.m.}}, J) P_{\mathrm{CN}}(E_{\mathrm{c.m.}}, J) W_{\mathrm{sur}}(E_{\mathrm{c.m.}}, J) \tag{1}$$

where $E_{\mathrm{c.m.}}$ and J are the incident energy and angular momentum in the center of mass coordinate system. The σ_{cap}, P_{CN} and W_{sur} denote capture cross section, fusion probability and the survival probability, respectively.

The σ_{cap} is mainly calculated using the empirical coupled-channel approach. Different potential distribution functions are constructed based on different modes of coupling between the projectile and the target. They are divided into three different cases: a fusion reaction involving two spherical nuclei, reactions with two statically deformed nuclei, and reactions with the combination of one spherical nucleus and one statically deformed nucleus, as described in detail in the Ref. [39]. For a given center-of-mass energy $E_{\mathrm{c.m.}}$, the σ_{cap} ($E_{\mathrm{c.m.}}$,J) can be expressed as [40]:

$$\sigma_{\mathrm{cap}}(E_{\mathrm{c.m.}}, J) = \frac{\pi\hbar^2}{2\mu E_{\mathrm{c.m.}}} \sum_J (2J+1) T(E_{\mathrm{c.m.}}, J) \tag{2}$$

where μ denotes the reduced mass of the projectile and target nuclei. $T(E_{\mathrm{c.m.}}, J)$ is the penetration probability of the two colliding nuclei overcoming the Coulomb barrier in the entrance channel.

By numerically solving the four-variable master equations in the corresponding potential energy surface, the time evolution of the probability distribution function $P(Z_1, N_1, \beta_{12}, \beta_{22}, \theta_1, \theta_2, \varepsilon_1, \tau_{int})$ under the directional angles (θ_1 and θ_2) can be obtained, which are mentioned in detail in Ref. [41–43]. Finally, the fusion probability P_{CN} is given by

$$\begin{aligned} P_{\mathrm{CN}}(E_{\mathrm{c.m.}}, J) = \sum_{Z_1=1}^{Z_{BG}} \sum_{N_1=1}^{N_{BG}} \int_0^{\infty} \int_0^{\infty} \int_0^{\pi/2} \int_0^{\pi/2} \\ P(Z_1, N_1, \beta_{12}, \beta_{22}, \theta_1, \theta_2, \tau_{int}) \\ \rho_1(\beta_{12})\rho_2(\beta_{22}) \sin\theta_1 \sin\theta_2 d\beta_{12} d\beta_{22} d\theta_1 d\theta_2, \end{aligned} \tag{3}$$

where N_{BG} and Z_{BG} are the Businaro-Gallone points. $\rho_i(\beta_{i2})$=1/h_i denote the density of the discrete dots with the step length h_i (i=1,2). The interaction time τ_{int} in the dissipative process of two colliding nuclei is determined by the deflection function method [44].

The survival probability is important in evaluation of the cross section. In the de-excitation process of the compound nucleus, two different statistical models are employed for theoretical calculations: statistical model 1 and statistical model 2 (GEMINI++ model). In model 1, similar to neutron evaporation, the probability in the channel of evaporating the x-th neutron, the y-th proton and the z-th α particle is expressed as [45]

$$\begin{aligned} W_{\mathrm{sur}}(E^*_{\mathrm{CN}}, x, y, z, J) = P(E^*_{CN}, x, y, z, J) \\ \times \prod_{i=1}^{x} \frac{\Gamma_n(E^*_i, J)}{\Gamma_{tot}(E^*_i, J)} \prod_{j=1}^{y} \frac{\Gamma_p(E^*_j, J)}{\Gamma_{tot}(E^*_j, J)} \prod_{k=1}^{z} \frac{\Gamma_\alpha(E^*_k, J)}{\Gamma_{tot}(E^*_k, J)} \end{aligned} \tag{4}$$

Where $P(E^*_{\mathrm{CN}}, x, y, z, J)$ denotes the realization probability when the excitation energy of the compound nucleus is E^*_{CN} and its angular momentum is J. The total width Γ_{tot} for the CN decay is the sum of the partial widths of particle evaporation Γ_m ($m = n, p, \alpha$ for neutron, proton, α particle, respectively), γ-emission and fission Γ_f. The excitation energy E^*_s before evaporating the s-th particle is evaluated by

$$E^*_{s+1} = E^*_s - B^n_i - B^p_j - B^\alpha_k - 2T_s \tag{5}$$

with the initial condition $E^*_1 = E^*_{CN}$ and $s = i + j + k$. The B^n_i, B^p_j, B^α_k are the separation energy of the i-th neutron, j-th proton, k-th α particle, respectively [46]. The relationship between the compound nuclear temperature T_i and the excitation energy can be expressed as

$$E^*_i = aT^2_i - T_i \tag{6}$$

For one particle evaporation, the realization probability is given by

$$P(E^*_{\mathrm{CN}}, J) = \exp\left(-\frac{(E^*_{\mathrm{CN}} - B_s - 2T)^2}{2\sigma^2}\right). \tag{7}$$

Where σ is the value obtained by experimentally measuring the width of the excitation function based on the fusion evaporation reaction. The probability $P(E^*_{\mathrm{CN}}, x, y, z, J)$ of evaporating x-neutrons, y-protons, and z-α particles at the excitation energy E^*_{CN} and angular momentum J is calculated

using the Jackson formula [47].

$$P(E^*_{\rm CN}, s, J) = I(\Delta_s, 2s-3) - I(\Delta_{s+1}, 2s-1) \quad (8)$$

where the quantities I and Δ are given by as follows:

$$I(z, m) = \frac{1}{m!}\int_0^z u^m e^{-u} {\rm d}u \quad (9)$$

$$\Delta_s = \frac{E^*_{CN} - \sum_{i=1}^{s} B_i^\nu}{T_i} \quad (10)$$

Where the B_i^ν is the separation energy of the evaporation of the i-th particle and $s(x, y, z) = x + y + z$.

The particle decay widths are evaluated with the Weisskopf's evaporation theory [48] as

$$\begin{aligned}\Gamma_\nu(E^*, J) &= (2s_\nu + 1)\frac{m_\nu}{\pi^2\hbar^2\rho(E^*, J)} \\ &\times \int_0^{E^*-B_\nu-\delta-\delta_n-\frac{1}{a}} \varepsilon\rho(E^* - B_\nu - \delta_n - E_{rot} - \varepsilon, J) \\ &\times \sigma_{inv}(\varepsilon){\rm d}\varepsilon.\end{aligned} \quad (11)$$

Here, s_ν, m_ν and B_ν are the spin, mass and binding energy of the evaporating particle, respectively. The inverse cross section is given by $\sigma_{inv} = \pi R_\nu^2 T(\nu)$ with the radius of $R_\nu = 1.21[(A - A_\nu)^{1/3} + A_\nu^{1/3}]$, and A_ν is the mass number of the evaporated particle. The penetration probability is set to be unity for neutrons and $T(\nu) = (1 + \exp(\pi(V_C(\nu) - \varepsilon)/\hbar\omega))^{-1}$ for charged particles with $\hbar\omega$ = 5 and 8 MeV for proton and α, respectively. The coulomb barrier calculation in the case of emission of charge particles, which can be as

$$V_C = \frac{Z_{CN-i}Z_i e^2}{r_i(A_{CN-i}^{1/3} + A_i^{1/3})}. \quad (12)$$

Here, for proton emitting r_p = 1.7 fm, and for α emitting r_α = 1.75 fm, this is described in detail in Ref. [49].

The fission width can be calculated with the Bohr-Wheeler formula as [46, 50]

$$\begin{aligned}\Gamma_f(E^*, J) &= \frac{1}{2\pi\rho_f(E^*, J)}\int_0^{E^*-B_f-E_{rot}-\delta-\delta_f-\frac{1}{a_f}} \\ &\frac{\rho_f(E^* - B_f - \delta_f - E_{rot} - \varepsilon, J){\rm d}\varepsilon}{1 + \exp[-2\pi(E^* - B_f - \delta_f - E_{rot} - \varepsilon)/\hbar\omega]},\end{aligned} \quad (13)$$

Here, we take $\hbar\omega$ = 2.2 MeV for all the nuclei considered [51], δ_f is a correction for fission barrier. And B_f is the fission barrier, consisting of the macroscopic part and the microscopic part, more details are given in Ref. [46].

The level density is calculated using the back-shifted Fermi-gas model [52]. Replace the excitation energy with the equivalent excitation energy U = E-δ. The back-shifts δ = -Δ(odd-odd), 0(odd-A) and Δ(even-even), respectively, are related to the neutron and proton pairing gap $\Delta = 1/2[\Delta_n(Z, N) + \Delta_p(Z, N)]$. The energy level density is expressed as

$$\rho(U, J) = \frac{(2J+1)\exp\left[2\sqrt{aU} - \frac{J(J+1)}{2\sigma^2}\right]}{24\sqrt{2}\sigma^3 a^{1/4} U^{5/4}}, \quad (14)$$

with $\sigma^2 = \frac{\Theta_{rigid}}{\hbar^2}\sqrt{\frac{U}{a}}$, $\Theta_{rigid} = \frac{2}{5}m_u A R^2$.

The selection of the level-density parameter in Eq. (14) is crucial, as it should be applied to both low and high excitation energy regions. Only in this way the statistical model 1 can be more rationally utilized to describe the de-excitation and fission processes of nuclei in the excited state. It is closely related to the excitation energy of the nucleus and the shell correction.

$$a(U, Z, N) = \tilde{a}(A)\left[1 + E_{\rm sh}\frac{f(U)}{U}\right] \quad (15)$$

$$\tilde{a}(A) = \alpha A + \beta A^{2/3} \quad (16)$$

$$f(U) = 1 - \exp(-\gamma_D U) \quad (17)$$

The $\tilde{a}(A)$ is the asymptotic Fermi-gas value of the level density parameter at high excitation energy. It is worth noting that in Fermi gas models of the same type, different density of states parameters mainly depend on the different shell corrections chosen. Under the condition that the shell corrections are given by a certain mass formula, the values in the energy level density parameters are finally extracted by fitting all nuclei with experimental values of energy level densities. In this paper, the microscopic shell corrections from FRDM95 [53] are used to fit the experimental level density data, resulting in parameters α = 0.1337, β=-0.06571, γ_D= 0.04884 [54].

Another statistical model we used in this work is GEMINI++, which is the improved version of the GEMINI statistical decay model, developed by R. J. Charity [55] to describe the formation of complex-fragment in heavy ion fusion experiments. The de-excitation of a compound nucleus occurs through a series of binary decays until particle emission is energetically forbidden or impossible due to competition with γ-ray emission. The evaporation process of light particles is described using the Hauser-Feshbach model in GEMINI++. In the statistical model 1 and GEMINI++ model, the same fission barrier is used. However, there are differences in the calculation methods for the fission widths. In the GEMINI++ model, the Bohr-Wheeler formulism is used forsymmetric fission [56]. For mass asymmetric fission outside the symmetric fission peak, the Moretto formulism is used. For statistical model 1, only Bohr-Wheeler's formula is used. Additionally, there are differences in the treatment of level density and the parameters of level density between the two models. In GEMINI++, the level density is calculated using the Fermi gas model:

$$\rho(E^*, J) \sim \exp(2\sqrt{a(U)U}). \quad (18)$$

The level density parameter $\tilde{a}(U)$ is also related to the excitation energy and it is given by:

$$\tilde{a}(U) = \frac{A}{k_\infty - (k_\infty - k_0)\exp(-\frac{\kappa}{k_\infty - k_0}\frac{U}{A})}. \quad (19)$$

The parameter κ defines how fast the long-range correlations wash out with excitation energy. But the fitting range of κ is small, and the maximum compound nucleus is only A = 224 [57]. The de-excitation process of this work is simulated using the GEMINI++ model and the default parameters of this model are used for the calculations.

III. NUMERICAL RESULTS AND DISCUSSIONS

A. Production cross sections of heavy isotopes in ^{40}Ar induced reactions

A variety of new nuclides have been successfully synthesized in the proton-rich region. Nevertheless, there are still many unknown nuclides in this region waiting to be explored. To further evaluate the potential of ^{40}Ar beam in the synthesis of new nuclides, we will continue to use ^{40}Ar as the projectile to bombard different targets in subsequent theoretical calculations. The ERCSs for the ^{40}Ar-induced reactions with the target nuclei ^{144}Sm, ^{160,164}Dy, ^{165}Ho, ^{166}Er, ^{169}Tm, ^{171,174}Yb, ^{175}Lu, $^{176-180}$Hf, ^{181}Ta, ^{180,182}W and ^{187}Re are presented in Figs. 1-5, and compared them with the available experimental data [18, 19, 21, 22, 58–60]. In order to ensure the reliability of the calculations, the same set of models and parameters should be used to calculate the reaction systems for all the projectile-target combinations in this work.

The survival probabilities, calculated for two different statistical model, are shown in Figs. 1-5 for comparison. The solid lines indicate cross sections calculated via the DNS + statistical model 1, the dashed lines indicate cross sections derived using the DNS + GEMINI++ model, and hollow symbols indicate the relevant experimental data. The difference is that in Figs. 1-2 there is only the evaporation of pure neutrons and in Figs. 3-5 the evaporation of charged particles is included.

As can be seen in Fig. 1, the calculated results obtained by DNS + statistical model 1 and the DNS + GEMINI++ model are in good agreement with the experimental data. The errors between the theoretical ERCSs and the experimental data are basically within 1 order of magnitude. Fig. 2 show the ERCSs for the ^{180}W(^{40}Ar, xn)$^{220-x}$U, ^{182}W(^{40}Ar, xn)$^{222-x}$U, ^{187}Re(^{40}Ar, xn)$^{227-x}$Np reactions. The computational results based on statistical model 1 are close to the relevant experimental data. However, when utilizing the GEMINI++ model to calculate the survival probability, a noticeable deficiency emerges in the form of a lower number of events in the neutron evaporation channels. This indicates that the GEMINI++ model has certain limitations in some reaction systems. By comprehensively comparing the theoretical calculation results of the two different models in these reactions, we can conclude that the results derived from both models are not significantly different and the statistical model 1 has a wider range of applicability.

To investigate the effect of different de-excitation processes of evaporating neutrons and charged particles on the ERCSs, we analyze different evaporation channels of the ^{40}Ar+^{171,174}Yb, $^{176-180}$Hf, ^{175}Lu, ^{181}Ta reactions in Figs. 3-5. In general, the production of certain isotopes is more likely in the xn evaporation channel. However, the pxn and αxn evaporation channels allow us to obtain access to those isotopes which are unreachable in the xn channels due to the lack of proper projectile-target combination, this is discussed in detail by Juhee Hong et al [61]. It provides a new perspective for the synthesis of some new nuclides.

It can be seen from Figs. 3-5, for most channels of pure neutron evaporation, the DNS + statistical model 1 calculates cross sections that are 1-2 orders of magnitude higher than those of DNS + GEMINI++ model. There is a difference of about 1-2 orders of magnitude between the statistical model 1 and the experimental data, while the DNS + GEMINI++ model calculations are within 1 order of magnitude of the experimental data. In the pxn evaporation channel, the computational results of the two models are not very different and both are in good agreement with the experimental data. In the αxn evaporation channel, cross sections calculated using DNS + GEMINI++ show a significantly better agreement with the experimental data than those calculated using DNS + statistical model 1. Overall, in the αxn evaporation channels, cross sections from the DNS + GEMINI++ model perform better than those from the DNS + statistical model 1.

By comparing ERCSs of the pure neutron evaporation channels and the charged particle evaporation channels (pxn and αxn) from Figs. 3-5, it is found that for the same projectile-target combination, the differences in ERCSs are mainly caused by different de-excitation modes. Specifically, these differences are mainly attributed to the survival probability. Moreover, the ERCSs in the proton evaporation channels are typically smaller than those in the neutron evaporation channel, with the α particle evaporation channel having the smallest cross sections. This may be due to the fact that protons and α particles have higher separation energies and Coulomb potential barriers ($B_P > B_n$), and they need to overcome a larger Coulomb barrier during the evaporation process, which results in relatively smaller cross sections.

It is worth noting that, based on Figs. 1-5, there are certain discrepancies between the theoretical calculations and experimental data for some evaporation channels. These differences are caused by a combination of experimental errors and uncertainties in theoretical calculations. On the experimental side, accelerators cannot provide precise incident energies but rather a variance around that value. Additionally, the precise measurement of ERCSs is also challenging, so the measured ERCSs usually have upper and lower error limits. On the theoretical side, our model requires a potential energy surface as input when calculating fusion probabilities [62, 63]. However, the calculation of the multidimensional potential energy surface for the reaction system is a complicated physical problem, which has not yet been fully solved. And the dependency of the fusion probability on excitation energy and the reaction entrance channel is not well established. In addition, survival probability are calculated based on certain nuclear data, such as nuclear masses, neutron separation energies, and fission barriers (shell correction energies), which are usually extrapolated. For instance, in the calculation of the cross sections for hot fusion reactions to synthesize superheavy nuclei,

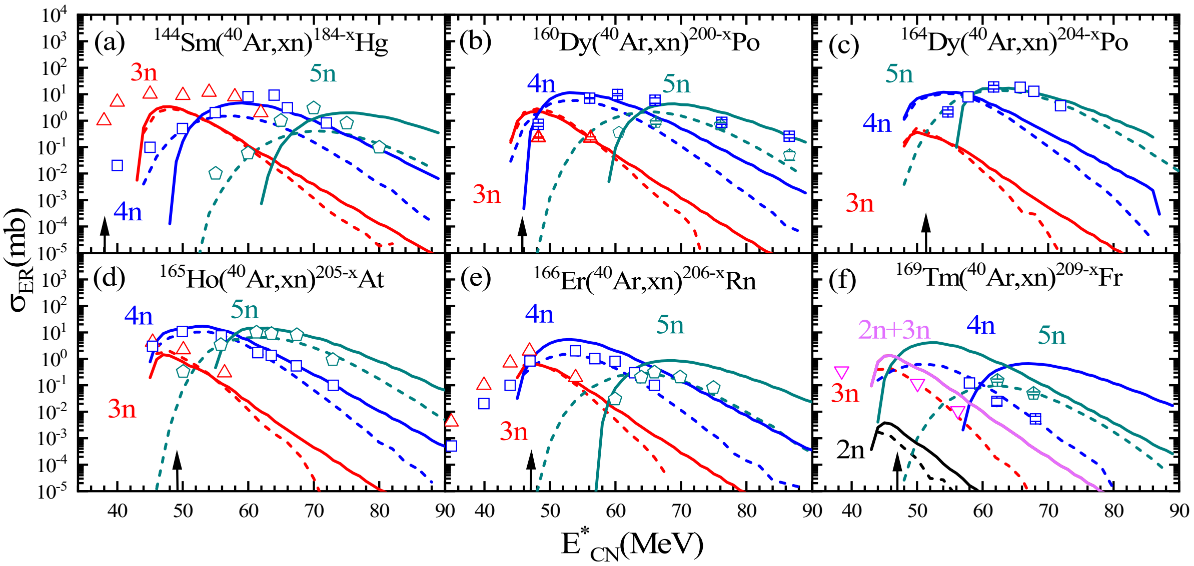

Fig. 1. (Color online) The ^{144}Sm, ^{160}Dy , ^{164}Dy, ^{165}Ho, ^{166}Er, ^{169}Tm targets were bombarded with ^{40}Ar projectile, the solid line indicates the cross sections calculated with the DNS + statistical model 1, and the dashed part indicates the cross sections derived using the DNS + GEMINI++ model. The different channels 2n, 3n, 4n, 5n, 2n+3n are represented by black, red, blue, dark cyan and pink, and the corresponding experimental data [58–60] are represented by hollow square up-triangles(3n), squares(4n), pentagons(5n) and down-triangles(2n+3n) respectively. The arrows show positions of the corresponding Bass barriers.

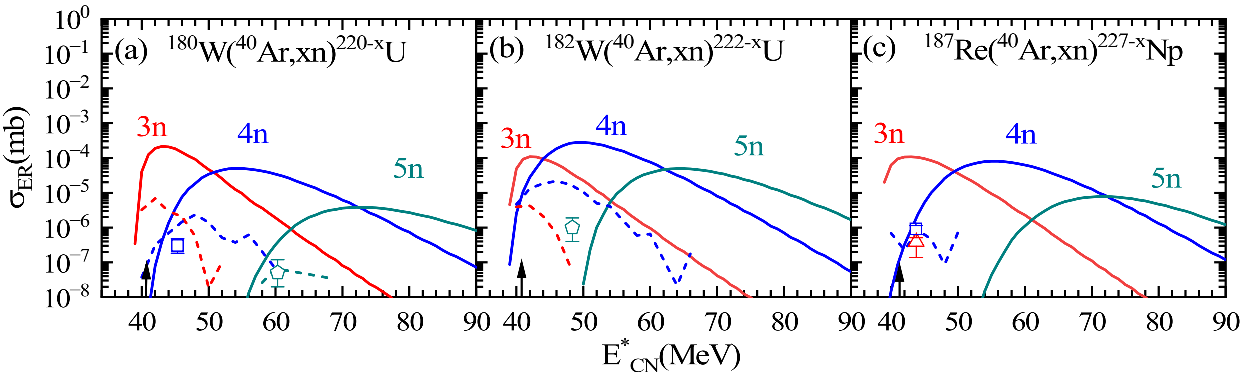

Fig. 2. (Color online) The ^{180}W, ^{182}W and ^{187}Re targets were bombarded with ^{40}Ar projectile, the solid line indicates the cross sections calculated with the DNS + statistical model 1, and the dashed part indicates the cross section derived using the DNS + GEMINI++ model. The different channels 2n, 3n, 4n, 5n are represented by black, red, blue and dark cyan, and the corresponding experimental values [18, 19, 21, 22] are represented by hollow up-triangles(3n), squares(4n) and pentagons(5n) respectively.

the compound nucleus will evaporate 3-4 neutrons, at which point the precision of the fission barrier is critical. When the height of the fission barrier is imprecise, the calculation errors in the neutron decay width and the ratio of fission width to (xn) de-excitation cascade at each step will accumulate, leading to an increased calculation error in the synthesis cross sections [64].

Research has revealed that the production of new nuclides in the superheavy region is primarily through the evaporation of neutrons. The previous discussion shows that two de-excitation models give similar results in the pure neutron evaporation channels. As mentioned in Ref. [65], it found that the GEMINI++ model is able to better represent the survival process in the Z = 82-92 nuclear region and it also identified limitations of the GEMINI++ model in calculating survival probabilities in the actinide and superheavy nuclei regions. In addition, the number of simulations required is substantial, especially in the superheavy region where it reaches 1,000,000. Using the GEMINI++ model to simulate the de-excitation process is time-consuming. So we have chosen to use statistical model 1 for the generation of cross section prediction in the following parts B and C.

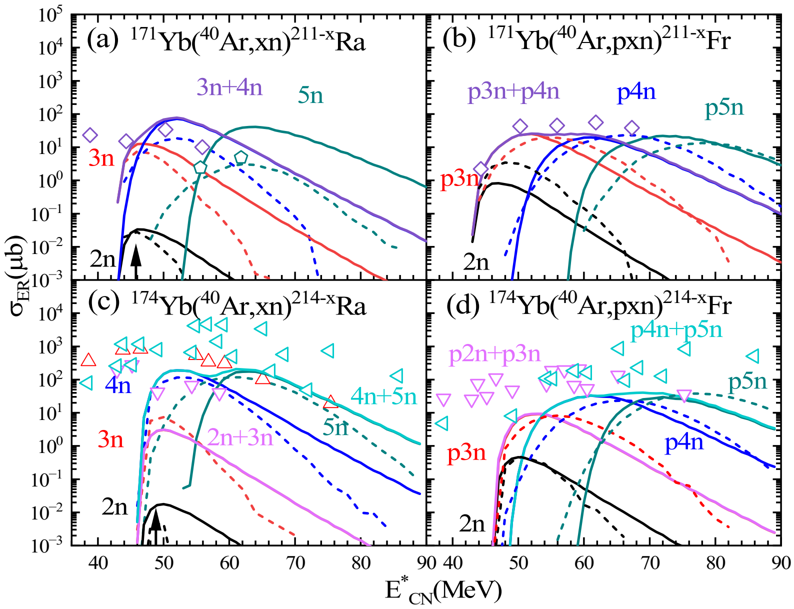

Fig. 3. (Color online) The ^{171,174}Yb isotopes were bombarded with ^{40}Ar projectile, the solid lines indicates the ERCSs calculated with the DNS + statistical model 1, and the dashed lines indicates the ERCSs derived using the DNS + GEMINI++ model. The different channels 2n, 3n, 4n, 5n, 2n+3n, 3n+4n and 4n+5n are represented by black, red, blue, dark cyan, pink, purple and cyan, and the corresponding experimental data [58, 60]are represented by hollow pentagons(5n), down-triangles(2n+3n), rhombus(3n+4n) and left-triangles(4n+5n) respectively.

B. Production cross sections of Pu, Cm, Bk proton-rich isotopes in the heavy nuclear region

Based on the reliability of theoretical calculations and to explore the potential of ^{40}Ar in synthesizing new isotopes, we will continue to use ^{40}Ar as the incident particle to further predict the ERCSs of new nuclides that could potentially be synthesized in the laboratory. Regarding the selection of ^{184}Os, ^{192}Pt and ^{197}Au as target materials, the primary reasons are as follows. Firstly, these targets possess long half-lives, which ensures their stability over extended periods during experiments, enhancing efficiency and data reliability. Furthermore, when the ^{40}Ar beam bombards these target nuclei under the current experimental conditions, there is a possibility of producing new nuclides that lie beyond the existing proton drip line. Fig. 6 shows the relevant theoretical calculations obtained by the DNS + statistical model 1.

As can be seen from Fig. 6, for the ^{184}Os (^{40}Ar, xn) $^{224-x}$Pu reaction system, the maximum cross sections of 3n, 4n and 5n channels are 266.27, 176.53 and 31.63 pb, respectively, resulting in the production of $^{219-221}$Pu, and the maximum ERCS is located in the 3n channel, corresponding to the excitation energy of approximately 45 MeV. The maximum cross sections of 3n, 4n and 5n channels for ^{192}Pt (^{40}Ar, xn) $^{232-x}$Cm reaction are 177.34, 40.94 and 5.54 pb, respectively, resulting in the production of $^{227-229}$Cm. The maximum ERCS is located in 3n channel, and the corresponding excitation energy is about 47 MeV. For ^{197}Au (^{40}Ar, xn) $^{237-x}$Bk reaction system, the maximum cross sections of 3n, 4n and 5n channels are 3193.41, 376.49 and 54.77 pb, respectively, resulting in the production of $^{232-234}$Bk. The maximum ERCS is located in 3n channel, and the corresponding excitation energy is around 45 MeV.

C. Production cross sections of Ds, Cn, Fl proton-rich isotopes in the superheavy nuclear region

Similarly, we also predict the ERCSs of new nuclides in the superheavy nuclear regions that may be synthesized in the laboratory. In this study, ^{40}Ar is utilized as the projectile to bombard actinide targets, including ^{238}U, ^{244}Pu, and ^{248}Cm. In the field of superheavy nuclei research, ^{238}U, ^{244}Pu and ^{248}Cm are commonly used target nuclei, which have been validated by numerous experiments, particularly those involving ^{48}Ca beams. These studies have yielded invaluable data for understanding the properties of superheavy elements.

Fig. 7(a) shows the predicted excitation function of xn ERCSs for the reaction ^{238}U (^{40}Ar, xn) $^{278-x}$Ds. The maximal ERCSs of the 3n, 4n and 5n channels are 1.479, 4.813 and 0.188 pb, respectively, resulting in the production of $^{273-275}$Ds. The largest ERCS is located in the 4n channel, with the corresponding excitation energy being 46 MeV. Especially noteworthy is the new nuclide ^{273}Ds, which was produced through the combination of ^{40}Ar + ^{238}U with a production cross sections of σ = 0.18 pb at the excitation energy of 49 MeV [23]. There is a 2.67 times difference compared to the theoretically result of 0.48 pb. In Fig. 7 (b), the maximum cross sections of the 3n, 4n and 5n channels of the ^{244}Pu(^{40}Ar, xn) $^{284-x}$Cn reaction are 1.215, 0.897 and 0.019pb, respectively, resulting in the production of $^{279-281}$Cn. The largest ERCS is located in the 3n chan-

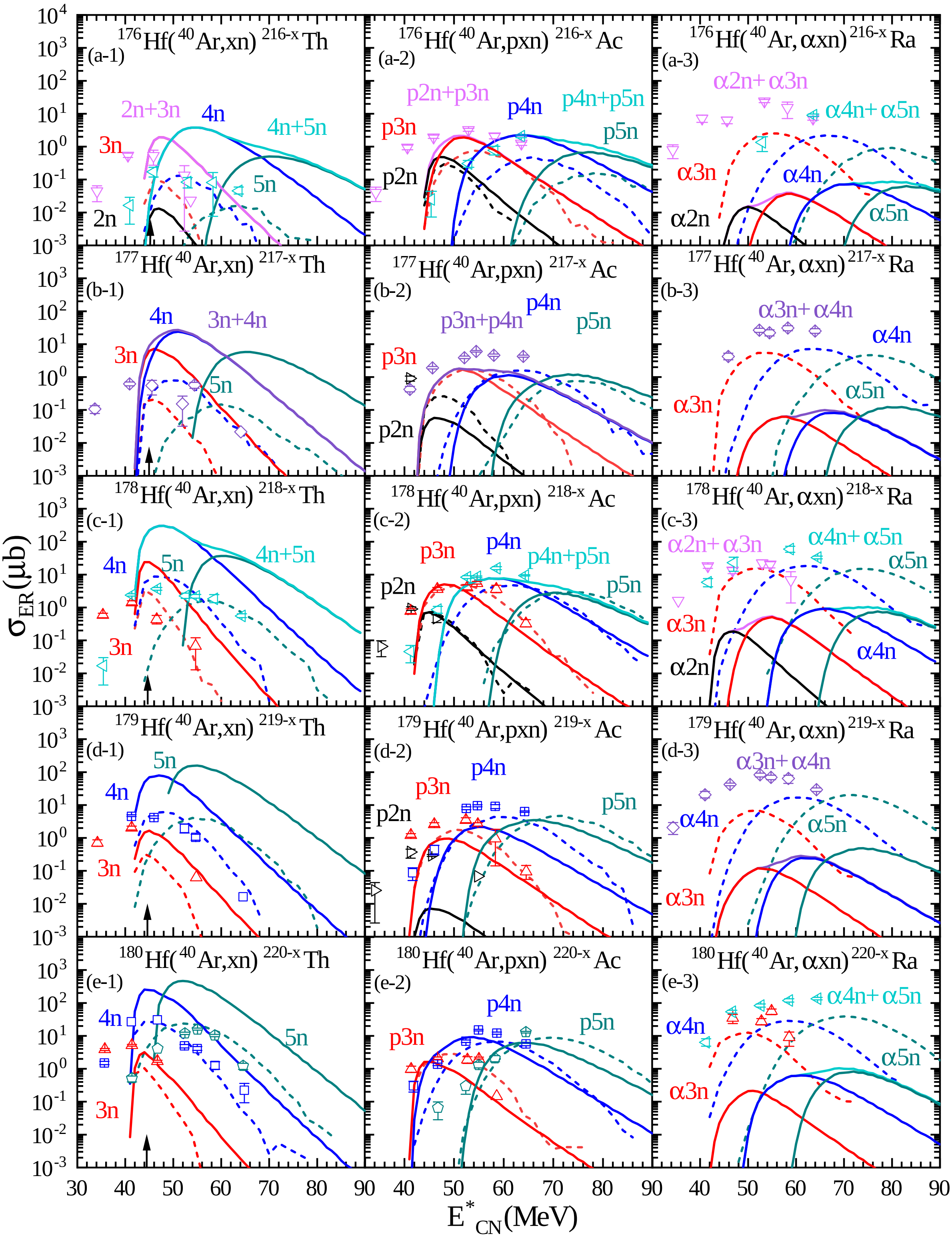

Fig. 4. (Color online) The $^{176-180}$Hf isotopes were bombarded with ^{40}Ar projectile, the solid lines indicates the ERCSs calculated with the DNS + statistical model 1, and the dashed lines indicates the ERCSs derived using the DNS + GEMINI++ model. The different channels 2n, 3n, 4n, 5n, 2n+3n, 3n+4n and 4n+5n are represented by black, red, blue, dark cyan, pink, purple and cyan, and the corresponding experimental values [58]are represented by hollow right-triangles(2n), up-triangles(3n), squares(4n), pentagons(5n), down-triangles(2n+3n), rhombus(3n+4n) and left-triangles(4n+5n) respectively.

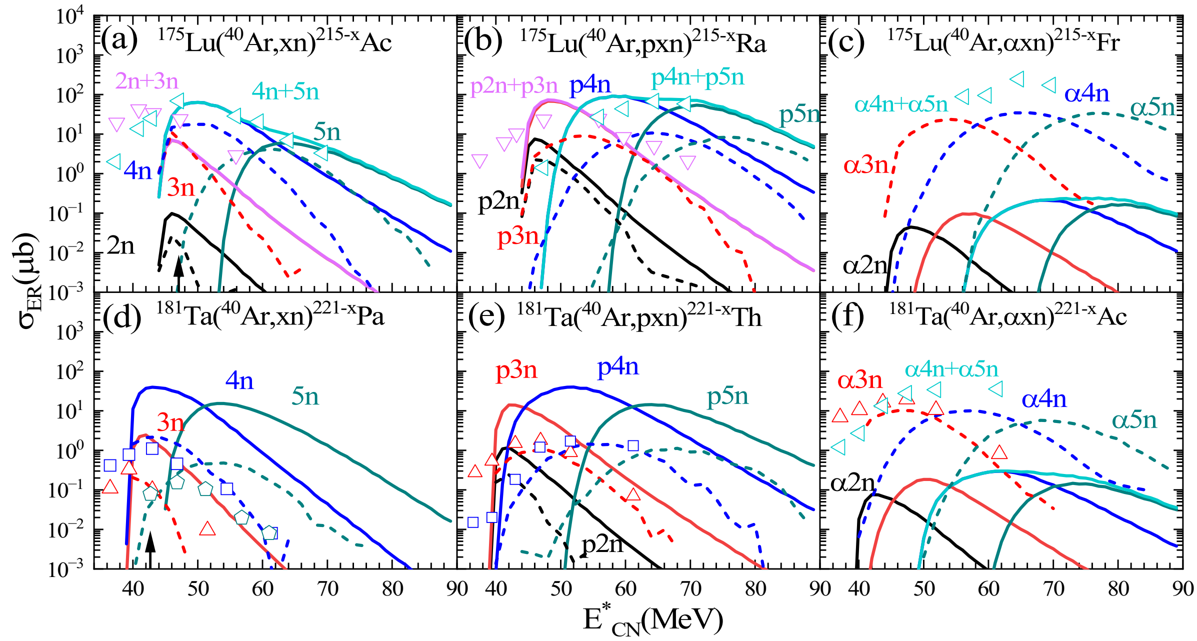

Fig. 5. (Color online) The ^{175}Lu and ^{181}Ta targets were bombarded with ^{40}Ar projectile, the solid lines indicates the ERCSs calculated with the DNS + statistical model 1, and the dashed lines indicates the ERCSs derived using the DNS + GEMINI++ model. The different channels 2n, 3n, 4n, 5n, 2n+3n and 4n+5n are represented by black, red, blue, dark cyan, pink and cyan, and the corresponding experimental data [58]are represented by hollow up-triangles(3n), squares(4n), pentagons(5n), down-triangles(2n+3n), rhombus(3n+4n) and left-triangles(4n+5n) respectively.

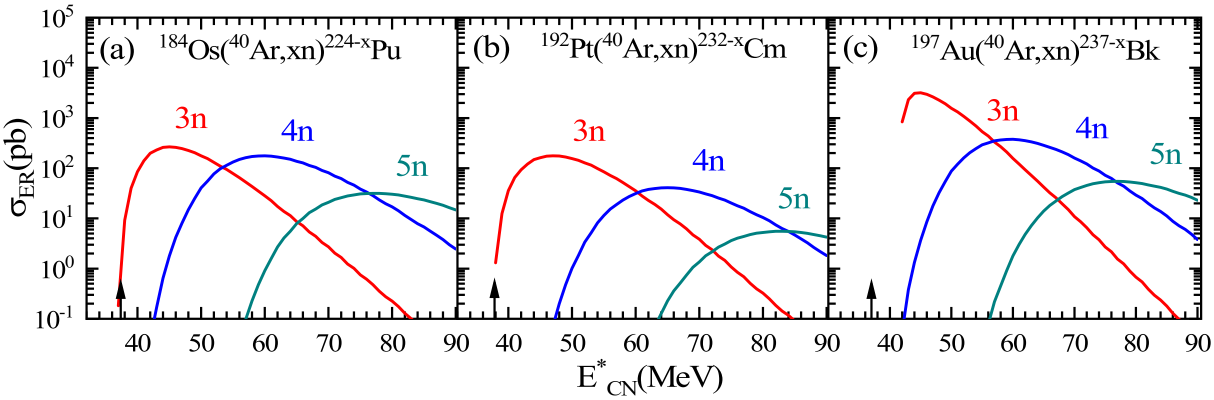

Fig. 6. (Color online) The ^{184}Os, ^{192}Pt, ^{197}Au were bombarded with ^{40}Ar projectile, the solid part indicates the ERCSs calculated with the DNS + statistical model 1. The different channels 3n, 4n and 5n are represented by red, blue and dark cyan, respectively.

nel, and its corresponding excitation energy is about 43 MeV. Similarly, for the ^{248}Cm (^{40}Ar, xn) $^{288-x}$Fl reaction system in Fig. 7 (c), the maximum cross section of 3n, 4n and 5n channels are 1.142, 2.699 and 0.071pb, respectively, resulting in the production of $^{283-285}$Fl and the maximum residual evaporation cross section is located in the 4n channel, corresponding to the excitation energy of approximately 45 MeV. The new nuclides such as $^{273-275}$Ds, ^{280,281}Cn, ^{284,285}Fl being the most probable isotopes owing to the current experimental detection limit of 0.1 pb [4].

IV. SUMMARY

Despite the fact that many areas of the nuclide chart have been filled in recent years, there are still many unknown nuclides in the proton drip line region. In order to search for proton-rich isotopes in heavy and superheavy regions, we have systematically investigated the ^{40}Ar-induced fusion evaporation reaction in the theoretical framework of the DNS model. In the calculation of survival probabilities, two different statistical models were employed. The results indicated no significant differences between the two models in the computations for neutron and proton evaporation chan-

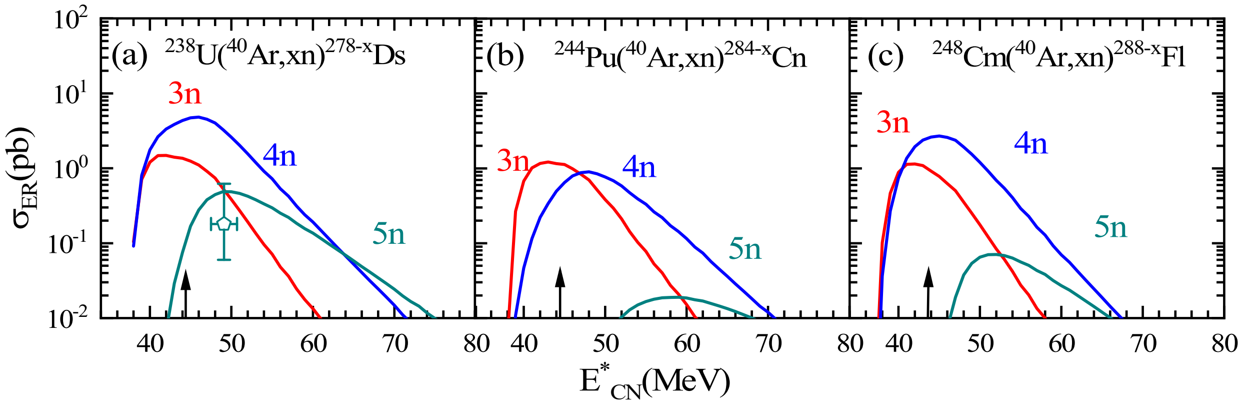

Fig. 7. (Color online) The ^{238}U, ^{244}Pu, ^{248}Cm were bombarded with ^{40}Ar projectile, the solid lines indicate the ERCSs calculated with the DNS + statistical model 1. The different channels 3n, 4n and 5n are represented by red, blue and dark cyan, respectively. The relevant experimental data[23] for the ^{238}U(^{40}Ar,5n)^{273}Ds are represented by hollow pentagons.

nels. However, the GEMINI++ model showed superior performance in the calculations for α-particle evaporation channels. But statistical model 1 is more broadly applicable. Based on statistical model 1, we used ^{40}Ar as the projectile to predict the ERCSs of new isotopes of actinide elements such as Pu, Cm and Bk. And the cross sections of new isotopes of Ds, Cn and Fl are predicted in the superheavy nuclei region of Z$\geq$104. The production cross sections of $^{273-275}$Ds, $^{279-281}$Cn, $^{283-285}$Fl are 0.488, 4.813, 1.479 pb; 0.019, 0.89, 0.215 pb; 0.071, 2.699, 1.142 pb, respectively. Because the current experimental limit is 0.1 Pb, $^{273-275}$Ds, ^{280,281}Cn, ^{284,285}Fl are more likely to be detected. We hope these results could inspire further synthesize studies of new isotopes in experiments.

---

[1] S. A. Giuliani, Z. Matheson, W. Nazarewicz *et al.*, Colloquium: Superheavy elements: Oganesson and beyond, Rev. Mod. Phys. **91**, 011001 (2019). https://doi.org/10.1103/RevModPhys.91.011001

[2] X. J. Bao, Y. Gao, J. Q. Li *et al.*, Theoretical study of the synthesis of superheavy nuclei using radioactive beams, Phys. Rev. C **91**, 064612 (2015). https://doi.org/10.1103/PhysRevC.91.064612

[3] S. Hofmann, G. Münzenberg, The discovery of the heaviest elements, Rev. Mod. Phys. **72**, 733 (2000). https://doi.org/10.1103/RevModPhys.72.733

[4] S. Hofmann, Super-heavy nuclei, J. Phys. G: Nucl. Part. Phys. **42**, 114001 (2015). https://doi.org/10.1088/0954-3899/42/11/114001

[5] S. Hofmann *et al.*, New results on elements 111 and 112, Eur. Phys. J. A. **14**, 147 (2002). https://doi.org/10.1140/epja/i2001-10119-x

[6] K. Morita *et al.*, Experiment on Synthesis of an Isotope ^{277}112 by ^{208}Pb + ^{70}Zn Reaction, J. Phys. Soc. Jpn. **76**, 043201 (2007). https://doi.org/10.1143/JPSJ.76.043201

[7] Yu. T. Oganessian *et al.*, Eleven new heaviest isotopes of elements Z=105 to Z=117 identified among the products of ^{249}Bk + ^{48}Ca reactions, Phys. Rev. C **83**, 054315 (2011). https://doi.org/10.1103/PhysRevC.83.054315

[8] Yu. T. Oganessian *et al.*, Investigation of the ^{243}Am + ^{48}Ca reaction products previously observed in the experiments on elements 113, 115, and 117, Phys. Rev. C **87**, 014302 (2013). https://doi.org/10.1103/PhysRevC.87.014302

[9] Yu. T. Oganessian, V. K. Utyonkov, Super-heavy element research, Rep. Prog. Phys. **78**, 036301 (2015). https://doi.org/10.1088/0034-4885/78/3/036301

[10] V. K. Utyonkov *et al.*, Experiments on the synthesis of superheavy nuclei ^{284}Fl and ^{285}Fl in the ^{239,240}Pu + ^{48}Ca reactionsPhys. Rev. C **92**, 034609 (2015). https://doi.org/10.1103/PhysRevC.92.034609

[11] E. M. Holmbeck, T. M. Sprouse,M. R. Mumpower, Nucleosynthesis and observation of the heaviest elements, Eur. Phys. J. A. **59**, 28 (2023). https://doi.org/10.1140/epja/s10050-023-00927-7

[12] B. Lommel, C. E. Düllmann, B. Kindler, D. Renisch, Status and developments of target production for research on heavy and superheavy nuclei and elements, Eur. Phys. J. A. **59**, 14 (2017). https://doi.org/10.1140/epja/s10050-023-00919-7

[13] G. M. Ter-Akopian, A. S. Iljinov, Y. T. Oganessian, O. A. Orlova *et al.*, Synthesis of the new neutron-deficient isotopes ^{250}102, ^{242}Fm, and ^{254}Ku, Nucl. Phys. A **255**, 509 (1975). https://doi.org/10.1016/0375-9474(75)90696-X

[14] G. Münzenberg, S. Hofmann, W. Faust, F.P. Heßberger *et al.*, The new isotopes ^{247}Md,^{243}Fm,^{239}Cf, and investigation of the evaporation residues from fusion of ^{206}Pb,^{208}Pb, and^{209}Bi with ^{40}Ar, Z. Phys. A **302**, 7 (1981). https://doi.org/10.1007/BF01425097

[15] V. Ninov, F.P. Heßberger, S. Hofmann, H. Folger, G. Münzenberg *et al.*, Identification of new mendelevium and einsteinium isotopes in bombardments of ^{209}Bi with ^{40}Ar, Z. Phys. A **356**, 11 (1996). https://doi.org/10.1007/s002180050141

[16] J. Khuyagbaatar, S. Hofmann, F.P. Heßberger, D. Ackermann *et al.*, Spontaneous fission of neutron-deficient fermium isotopes and the new nucleus ^{241}Fm, Eur. Phys. J. A. **37**, 177 (2008). https://doi.org/10.1140/epja/i2008-10608-4

[17] O.N. Malyshev, A.V. Belozerov, M.L. Chelnokov et al. The new isotope ^{217}U, Eur. Phys. J. A **8**, 295 (2000). https://doi.org/10.1007/s100500070082

[18] L. Ma et al., α-decay properties of the new isotope ^{216}U, Phys. Rev. C **91**, 051302 (2015). https://doi.org/10.1103/PhysRevC.91.051302

[19] H.B. Yang, Z.Y. Zhang, J.G. Wang, Z.G. Gan, Alpha decay of the new isotope ^{215}U, Eur. Phys. J. A **51**, 88 (2015). https://doi/10.1140/epja/i2015-15088-9

[20] Z.Y. Zhang, Z. G. Gan, H. B. Yang *et al.*, New Isotope ^{220}Np: Probing the Robustness of the N=126 Shell Closure in Neptunium, Phys. Rev. Lett. **122**, 192503 (2019). https://doi.org/10.1103/PhysRevLett.122.192503

[21] M.D. Sun, Z. Liu, T.H. Huang et al., New short-lived isotope ^{223}Np and the absence of the Z = 92 subshell closure near N = 126, Phys. Lett. B **771**, 303 (2017). https://doi.org/10.1016/j.physletb.2017.03.074

[22] T. H. Huang, W. Q. Zhang, M. D. Sun et al., Identification of the new isotope ^{224}Np. Phys. Rev. C **98**, 044302 (2018). https://doi.org/10.1103/PhysRevC.98.044302

[23] Y. T. Oganessian, V. K. Utyonkov, M. V. Shumeiko, F. S. Abdullin, G. G. Adamian, Synthesis and decay properties of isotopes of element 110: ^{273}Ds and ^{275}Ds, Phys. Rev. C **109**, 054307 (2024). https://doi.org/10.1103/PhysRevC.109.054307

[24] S. Bjrnholm, W. J. Swiatecki, Dynamical aspects of nucleus-nucleus collisions, Nucl. Phys. A. **391**, 471 (1982). https://doi.org/10.1016/0375-9474(82)90621-2

[25] V. Zagrebaev, W. Greiner, Unified consideration of deep inelastic, quasi-fission and fusion–fission phenomena, J. Phys. G: Nucl. Part. Phys. **31**, 825 (2005). https://doi.org/10.1088/0954-3899/31/7/024

[26] V. Zagrebaev, Synthesis of superheavy nuclei: Nucleon collectivization as a mechanism for compound nucleus formation, Phys. Rev. C. **64**, 034606 (2001). https://doi.org/10.1103/PhysRevC.64.034606

[27] K. Zhao, Z. Li, Y. Zhang *et al.*, Production of unknown neutron-rich isotopes in ^{238}U + ^{238}U collisions at near-barrier energy, Phys. Rev. C **94**, 024601 (2016). https://doi.org/10.1103/PhysRevC.94.024601

[28] G. F. Dai, L. Guo, E. G. Zhao, S. G. Zhou, Dissipation dynamics and spin-orbit force in time-dependent Hartree-Fock theory, Phys. Rev. C **90**, 044609 (2014). https://doi.org/10.1103/PhysRevC.90.044609

[29] G. G. Adamian *et al.*, Fusion cross sections for superheavy nuclei in the dinuclear system concept, Nucl. Phys. A. **633**, 409 (1998). https://doi.org/10.1016/S0375-9474(98)00124-9

[30] G. G. Adamian, N.V.Antonenkoa *et al.*, Treatment of competition between complete fusion and quasifission in collisions of heavy nuclei, Nucl. Phys. A. **627**, 361 (1997). https://doi.org/10.1016/S0375-9474(97)00605-2

[31] X. J. Bao, Y. Gao, J. Q. Li, H. F. Zhang, Isotopic dependence of superheavy nuclear production in hot fusion reactions, Phys. Rev. C **92**, 034612 (2015). https://doi.org/10.1103/PhysRevC.92.034612

[32] L. Zhu, J. Su, Unified description of fusion and multinucleon transfer processes within the dinuclear system model, Phys. Rev. C. **104**, 044606 (2021). https://doi.org/10.1103/PhysRevC.104.044606

[33] N. Antonenko, E. Cherepanov, A. Nasirov, V. Permjakov, V. Volkov, Competition between complete fusion and quasi-fission in reactions between massive nuclei. The fusion barrier, Phys. Lett. B **319**, 425 (1993). https://doi.org/10.1016/0370-2693(93)91746-A

[34] N. V. Antonenko, E. A. Cherepanov, A. K. Nasirov, V. P. Permjakov, V. V. Volkov, Compound nucleus formation in reactions between massive nuclei: Fusion barrier, Phys. Rev. C **51**, 2635 (1995). https://doi/10.1103/PhysRevC.51.2635

[35] A. Diaz-Torres, G. G. Adamian, N. V. Antonenko, W. Scheid, Melting or nucleon transfer in fusion of heavy nuclei, Phys. Lett. B **481**, 228 (2000). https://doi.org/10.1016/S0370-2693(00)00471-8

[36] M. Huang, Z. Zhang, Z. Gan, X. Zhou, J. Li, W. Scheid, Dynamical deformation in heavy ion collisions and formation of superheavy nuclei, Phys. Rev. C **84**, 064619 (2011). https://doi/10.1103/PhysRevC.84.064619

[37] X. J. Bao, S. Q. Guo, H. F. Zhang *et al.*, Dynamics of complete and incomplete fusion in heavy ion collisions, Phys. Rev. C **97**, 024617 (2018). https://doi/10.1103/PhysRevC.97.024617

[38] G. Giardina, S. Hofmann, A.I. Muminov et al., Effect of the entrance channel on the synthesis of superheavy elements, Eur. Phys. J. A 8, 205–216 (2000). https://doi.org/10.1007/s10050-000-4509-7

[39] G. J. Li, X. J. Bao, Theoretical calculations for the capture cross section of the formation of heavy and superheavy nuclei, Phys. Rev. C **107**, 024611 (2023). https://doi.org/10.1103/PhysRevC.107.024611

[40] X. J. Bao, S. Q. Guo, H. F. Zhang, J. Q. Li, Influence of neutron excess of projectile on multinucleon transfer reactions, Phys. Lett. B **785**, 221 (2018). https://doi.org/10.1016/j.physletb.2018.08.049

[41] X. J. Bao, Production of light neutron-rich nuclei in multinucleon transfer reactions, Nucl. Phys. A **986**, 60 (2019). https://10.1016/j.nuclphysa.2019.02.009

[42] S. H. Zhu, T. L. Zhao, X. J. Bao, Systematic study of the synthesis of heavy and superheavy nuclei in ^{48}Ca-induced fusion-evaporation reactions, Nucl. Sci. Tech. **35**, 124 (2024). https://doi.org/10.1007/s41365-024-01483-5

[43] X. J. Bao, Possibility to produce ^{293,295,296}Og in the reactions ^{48}Ca + ^{249,250,251}Cf, Phys. Rev. C **100**, 011601(R) (2019). https://doi.org/10.1103/PhysRevC.100.011601

[44] C. Riedel, G. Wolschin, W. Noerenberg, Relaxation times in dissipative heavy-ion collisions, Z. Phys. A **290**, 47 (1979). https://doi.org/10.1007/BF01408479

[45] P. H. Chen, Z. Q. Feng, J. Q. Li *et al*, A statistical approach to describe highly excited heavy and superheavy nuclei, Chin. Phys. C **40**, 091002 (2016). https://10.1088/1674-1137/40/9/091002

[46] P. H. Chen, Production of proton-rich nuclei around Z = 84-90 in fusion-evaporation reactions, Eur. Phys. J. A. **53**, 95 (2017). https://doi.org/10.1140/epja/i2017-12281-x

[47] J. D. Jackson, A schematic model for (p, xn) cross sections in heavy elementa, Can. J. Phys. **34**, 767 (1956). https://doi.org/10.1139/p56-087

[48] V. Weisskopf, Statistics and Nuclear Reactions, Phys. Rev. 52, 295 (1937). https://doi.org/10.1103/PhysRev.52.295

[49] A. S. Zubov, G. G. Adamian, N. V. Antonenko, S. P. Ivanova, W. Scheid, Competition between evaporation channels in neutron-deficient nuclei, Phys. Rev. C **68**, 014616 (2003). https://doi.org/10.1103/PhysRevC.68.014616

[50] N. Bohr, J. A. Wheeler, The Mechanism of Nuclear Fission, Phys. Rev. **56**, 426 (1939). https://doi.org/10.1103/PhysRev.56.426

[51] A. S. Zubov, G. G. Adamian, N. V. Antonenko *et al.*, Survival probabilities of superheavy nuclei based on recent predictions of nuclear properties, Eur. Phys. J. A **23**, 249 (2005). https://doi.org/10.1140/epja/i2004-10089-5

[52] W. Dilg, W. Schantl, H. Vonach, Level density parameters for the back-shifted fermi gas model in the mass range 40 < A < 250, Nucl. Phys. A **217**, 269 (1973) https://doi.org/10.1016/0375-9474(73)90196-6

[53] P. Möller, J. R. Nix, W. D. Myers, *et al*., Nuclear Ground-State Masses and Deformations, Atom. Data Nucl. Data Tabl. **59**, 185 (1995). https://doi.org/10.1006/adnd.1995.1002

[54] T. Rauscher, F.K. Thielemann, K.L. Kratz, Nuclear level density and the determination of thermonuclear rates for astrophysics, Phys. Rev. C **56**, 1613 (1997). https://doi.org/10.1103/PhysRevC.56.1613

[55] R. J. Charity *et al*., Systematics of complex fragment emission in niobium-induced reactions, Nucl. Phys. A **483**, 371 (1988). https://doi.org/10.1016/0375-9474(88)90542-8

[56] D. Mancusi, R. J. Charity, J. Cugnon, Unified description of fission in fusion and spallation reactions, Phys. Rev. C **82**, 044610 (2010). https://doi.org/10.1103/PhysRevC.82.044610

[57] R. J. Charity, Systematic description of evaporation spectra for light and heavy compound nuclei, Phys. Rev. C **82**, 014610 (2010). https://doi.org/10.1103/PhysRevC.82.014610

[58] D.Vermeulen, H. G. Clerc, C. C. Sahm et al., Cross sections for evaporation residue production near the N=126 shell closure. Z. Physik A **318**, 157–169 (1984).https://doi.org/10.1007/BF01413464

[59] D. Kamas, A. Opichal, E. V. Chernysheva, S. N. Dmitriev et al., Evaporation-residue cross sections in complete fusion reactions leading to Hg and Rn isotopes, Phys. Rev. C **105**, 044612 (2022). https://doi.org/10.1103/PhysRevC.105.044612

[60] Y. LeBeyec, R. L. Hahn, K. S. Toth, R. Eppley., Reactions of ^{40}Ar with ^{160}Dy, ^{164}Dy, and ^{174}Yb, Phys. Rev. C **14**, 1038 (1976). https://doi.org/10.1103/PhysRevC.14.1038

[61] J. Hong, G. G. Adamian, N. V. Antonenko, Possibilities of production of transfermium nuclei in charged-particle evaporation channels, Phys. Rev. C **94**, 044606 (2016). https://doi.org/10.1103/PhysRevC.94.044606

[62] Z.H. Liu, J.D. Bao. Possibility to produce element 120 in the ^{54}Cr + ^{248}Cm hot fusion reaction. Phys. Rev. C **87**, 034616 (2013). https://doi.org/10.1103/PhysRevC.87.034616

[63] A. K. Nasirov, G. Mandaglio, G. Giardina, et al. Effects of the entrance channel and fission barrier in synthesis of superheavy element Z=120. Phys. Rev. C **84**, 044612 (2011). https://doi.org/10.1103/PhysRevC.84.044612

[64] K. Siwek-Wilczynska, T. Cap, M. Kowal, A. Sobiczewski, J. Wilczynski, Predictions of the fusion-by-diffusion model for the synthesis cross sections of Z=114–120 elements based on macroscopic-microscopic fission barriers, Phys. Rev. C **86**, 014611 (2012). https://doi.org/10.1103/PhysRevC.86.014611

[65] T.L.Zhao, S.H.Zhu, X.J.Bao, Analysis of the survival probability of super-asymmetric reaction systems based on the GEMINI++ model, unpublished